RESEARCH ARTICLE | DECEMBER 12 2024

Optical study of valence band splitting and resonant acceptor states in Cu_2GeS_3 microcrystals

Jüri Krustok ✉ ; Reelika Kaupmees ; Joel Kokla ; Marit Kauk-Kuusik

Appl. Phys. Lett. 125, 242111 (2024)
https://doi.org/10.1063/5.0245139

Applied Physics Letters ARTICLE pubs.aip.org/aip/apl

Optical study of valence band splitting and resonant acceptor states in Cu_2GeS_3 microcrystals

Cite as: Appl. Phys. Lett. **125**, 242111 (2024); doi: 10.1063/5.0245139
Submitted: 24 October 2024 · Accepted: 3 December 2024 ·
Published Online: 12 December 2024

View Online Export Citation CrossMark

Jüri Krustok,[a] Reelika Kaupmees, Joel Kokla, and Marit Kauk-Kuusik

AFFILIATIONS

Department of Materials and Environmental Technology, Tallinn University of Technology, Ehitajate tee 5, 19086 Tallinn, Estonia

[a]Author to whom correspondence should be addressed: Juri.Krustok@taltech.ee

ABSTRACT

Single microcrystals of Cu_2GeS_3 (CGS) were grown in molten LiI salt. According to x-ray diffraction measurements, all of the samples were made up entirely of CGS crystals. Raman spectra and photoluminescence (PL) at room temperature revealed two different types of crystals. Type A crystals displayed an asymmetric PL band at about 1.57 eV, while type B crystals displayed extra bands at 1.673, 1.587, and 1.474 eV. Raman spectra of both types were also different. The existence of two band-to-band recombinations, connected to split valence bands V1 and V2, is one explanation for the shape of the type B PL spectrum. It was discovered that the spin–orbit splitting energy was 0.11 eV. PL bands at 1.474 and 1.587 eV were related to acceptor levels coupled with V1 and V2 valence bands, respectively. For the V2 valence band, the depth of the resonant acceptor state was 0.09 eV. The acceptor level linked to the V1 valence band was also found to have the same value. To measure external quantum efficiency (EQE) spectra, monograin solar cells made from our microcrystals were used. The derivative of the EQE spectrum results in two distinct peaks, split by 0.11 eV. The inflection point minima are at 1.62 and 1.73 eV. We propose a model for various energy levels based on these findings.

In recent years, copper-based chalcogenides have attracted significant attention due to their potential applications in photovoltaic systems, optoelectronic devices, and photodetectors. Cu_2GeS_3 (CGS) is a ternary semiconductor that has become the focus of extensive research due to its exceptional combination of optical characteristics, tunable bandgap, and chemical stability. This material belongs to I2-IV-VI3 semiconductor family and crystallizes in a tetrahedrally coordinated structure similar to that of chalcopyrite.[1,2] Thanks to its intrinsic properties, Cu_2GeS_3 emerges as a promising alternative to traditional materials like silicon and gallium arsenide, particularly for thin-film solar cells and thermoelectric devices.[3] The optical characteristics of Cu_2GeS_3 are of special relevance due to their direct impact on the material's performance in optoelectronic applications. Its direct bandgap, typically ranging from 1.4 and 1.6 eV,[3] places it within the ideal range for effective visible light absorption, making it an excellent candidate for indoor photoluminescence (PV) applications or tandem PV cells.[4] Moreover, CGS exhibits p-type character and an absorption coefficient more than $10^4\ cm^{-1}$.[1]

Numerous studies have reported measurements of the Raman spectra of CGS.[4–9] The most intense Raman modes are detected at different wavenumbers, and although many modes are common, the peak intensity ratio varies across different phases. This is likely attributed to the unidentified compositions of the various crystal structures in the samples being examined. However, as it was shown in Ref. 5, CGS crystals may have different preferential orientations, so different Raman peaks would be observed from each crystal. Less research has been conducted on the photoluminescence characteristics of CGS crystals, although investigations at low temperatures have revealed very narrow PL bands and even excitonic emission.[6,8] The PL band at room temperature was discovered in monoclinic CGS thin films at 1.57 eV.[10] It was assumed that this PL band corresponds to the band-to-band transition. It is evident that further research is required to fully comprehend the optoelectronic characteristics of CGS crystals. The valence band splitting of CGS is one of these unresolved issues. The valence band spin–orbit splitting energy in CGS crystals ($\triangle_{SO} = -0.11$ eV) was first calculated in 1987.[11] External quantum efficiency (EQE) and absorption measurements in CGS thin films confirmed this value.[12] de Wild *et al.* performed a detailed analysis of the valence band splitting effect on the absorption spectra of monoclinic Cu_2GeS_3 by combining theoretical and experimental approaches.[13] They discovered that the

absorption spectra of thin films showed three distinct signatures, each corresponding to a different valence band. The distance between the uppermost valence band (V1) and the deeper band (V2) was 0.13 eV. However, theoretical calculations showed that the lowest valence band (V2) is actually split by 20 meV, leading to a slightly higher value for the spin-orbit valence band splitting. It was also demonstrated that the position of the V2 valence band could be found by calculating the derivative of the experimentally determined absorption coefficient, $d\alpha/dE$. Using a Tauc plot, the bandgap value was determined to be 1.51 eV.

The purpose of this work is to explore valence band splitting in Cu_2GeS_3 microcrystals produced in molten LiI salt using room temperature photoluminescence (RT-PL), EQE, and Raman spectroscopy.

Using the molten salt process, the commercially available Cu powder (99.999%, Alfa Aesar), Ge powder (99.999%, Alfa Aesar), and S powder (99.999%, Alfa Aesar) were combined to produce the ternary Cu_2GeS_3 microcrystalline powders. LiI (99.8%, Alfa Aesar) alkali salt was used as a molten salt medium (flux material). The mass ratio of $m_{precursors}$ to m_{flux} was 1:1. The mixture of precursors was degassed, sealed in quartz ampoules, and then heated from room temperature (RT) to 700 °C at a rate of ~0.5 °C/min, maintaining this temperature for 120 h. After the ampoules cooled to room temperature in the air, distilled water was used to leach the salt from the solid powder particles. Subsequently, the powder was dried at 50 °C in a hot-air oven. The resulting microcrystals had an average size of around 100 μm, see Fig. S1. Using the hot probe method, the microcrystals' conductivity type was identified as p-type. The polycrystalline powder was also synthesized in a different ampoule using the same temperature regimes. Using the Bruker EDX-XFlash 6/30 detector and an accelerating voltage of 20 kV, the bulk composition of the produced powder crystals was examined using energy dispersive x-ray spectroscopy (EDX) (the measurement error is around 0.5 at. %). It was found that bulk composition of the powder was slightly Cu-rich and Ge-poor ([Cu]/[Ge] > 2). The ratio of [S]/([Cu]+[Ge]) was approximately 1.0.

X-ray powder diffraction (XRD) was used to analyze the crystal structure of the Cu_2GeS_3 microcrystalline powder under study. The Rigaku Ultima IV diffractometer was equipped with a silicon strip detector D/teX Ultra and operated at 40 kV and 40 mA, producing monochromatic Cu Kα1 radiation ($\lambda = 1.5406$ Å). No evidence of secondary phases was found, according to XRD measurements. Cu_2GeS_3 is either orthorhombic (space group Imm2) or monoclinic (space group Cc) based on the powder's XRD patterns, see Fig. S2. Regretfully, it was difficult to distinguish one crystal phase from the other because the primary peaks for both of them occur at roughly the same angles. We presume that we most likely have a combination of the two phases.

Phase composition and μ-PL spectra of microcrystals were analyzed at room temperature by using a Horiba Lab-RAM HR800 micro-Raman system equipped with a cooled multichannel CCD detection system in the backscattering configuration with a spectral resolution better than 1 cm^{-1}. A YAG:Nd laser (wavelength $\lambda = 532$ nm) was used for Raman and PL excitation. The laser power density was around 90 kW/cm^2 due to the laser point size of approximately 2 μm in diameter. The ZnO/CdS/CGS monograin layer solar cells were fabricated from powder that had undergone thermal and chemical processing. This process is fully explained in our previous publications.[8,14,15] Following completion, the solar cells were subjected to optical measurements. Measurements of external quantum efficiency were carried out in the 350–1235 nm spectral range using an SPM-2 prism monochromator that was computer controlled. The produced photocurrent was observed at 0 V bias at RT by utilizing a 250 W halogen light.

In this investigation, over 50 distinct microcrystals were measured independently. The PL and Raman spectra were always measured from the same spot. These data mostly revealed the presence of two types of crystals: type A and type B. See Fig. 1 for details on how the Raman and PL properties varied somewhat for each type. Type A crystals makeup nearly 90% of crystals. Their PL intensity was higher, and they showed a weak contribution of BB2 recombination at about 1.68 eV, along with one asymmetric BB1 band that peaked at 1.565 eV.

The main Raman peaks were located at 273, 247, 395, 338, and 312 cm^{-1}. Type B crystals show additional PL bands at about 1.67 and 1.45 eV; see Fig. 1(b). Since the polycrystal sample also produced spectra of the same type, these extra bands cannot be linked to potential Li contamination from LiI salt, i.e., all Raman peaks belong to Cu_2GeS_3 lattice.

The primary peaks of type B crystals' Raman spectra are located at 395, 351, 318, and 295 cm^{-1}. For both crystal types, there are common peaks at 421, 395, 273, and 247 cm^{-1}. Our Raman spectra show good agreement with peaks found in two distinct crystals by Matsumoto *et al.*[5] Additionally, we discovered that crystal orientation under the polarized laser beam significantly affects the relative intensity of all Raman peaks but does not add any new peaks, see Fig. S3. This is a proof that our microcrystals are, indeed, perfect single crystals. See Fig. S4 for PL spectra of type B microcrystals, where the polarization effect was very similar but the spectra's overall shape remained

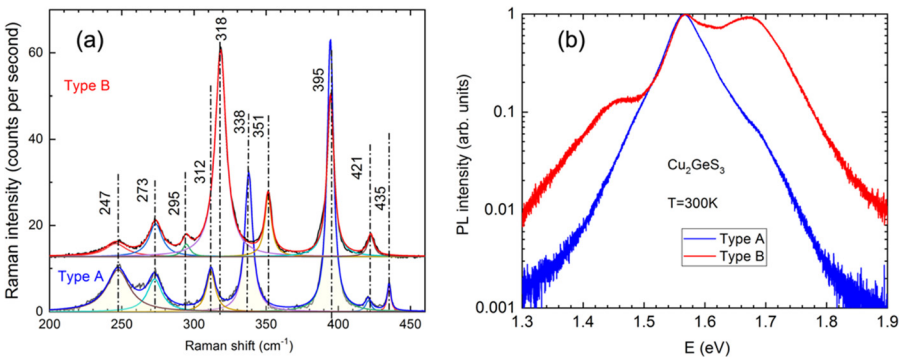

FIG. 1. Raman spectra (a) and normalized room temperature PL spectra (b) for the type A and type B Cu_2GeS_3 microcrystals.

unchanged. One possible explanation for the shape of the type B PL spectrum is the presence of two band-to-band recombinations, which are linked to split valence bands V1 and V2. About 0.1 eV separates the two higher energy PL bands, which is extremely near to the estimated values of 0.11–0.13 eV.[11,13] For type A crystal, a higher energy band at 1.68 eV is also noticeable, but it has very low intensity. The intrinsic defect level in type B crystal is most likely connected to the lower energy PL band at 1.45 eV. We carried out a spectral fitting to make the PL spectrum of the type B crystal more understandable, see Fig. 2. We used the asymmetric hyperbolic secant (AHS) function $I(E) = I_0/[\exp((E-E_M)/W_{HE}) + \exp(-(E-E_M)/W_{LE})]$ for band-to-band recombinations (BB1) and (BB2). Here, W_{HE} and W_{LE} correspond to the width of the high and low energy sides of the PL band, respectively, and E_M is related to the peak position E_{max}. The AHS function was selected because usually the shape of BB bands can be calculated as a product of $d(E)f(E)$, where $f(E)$ is a temperature dependent Fermi occupation function determining the high energy side of the BB band: $f(E) = \left[1 + \exp\left((E-E_F)/kT\right)\right]^{-1}$, and the density of states function $d(E)$ for direct bandgap semiconductors is a combination of two functions: $A\sqrt{2(E-E_G)/E_U}$ and $Aexp\left[\left((E-E_G)/E_U\right) - 1/2\right]$, where E_G is the width of the bandgap and E_U is the characteristic energy that scales the extent of the Urbach tail density of localized defect states in the gap. A is a global amplitude factor. The $d(E)$ function determines the low energy side of the BB bands. Figure 1(b) shows that the low energy side of BB bands has more or less exponential shape, and therefore, we expect that the Urbach tail part is dominating in the $d(E)$ function. Using the $d(E)$ function to fit the low-energy side of the BB band, we were able to determine the Urbach energy E_U, which came out to be 29 meV for the type A spectrum. The AHS function has been successfully used also to fit exciton emission in 2D materials.[16,17]

The best fitting was obtained by adding also two additional Gaussian bands, labeled A1 and A2. The fitting parameters are given in Table I, and the PL bands origin is specified in Fig. 2, inset. The BB2 band is observed to have a larger halfwidth than the BB1 band, which

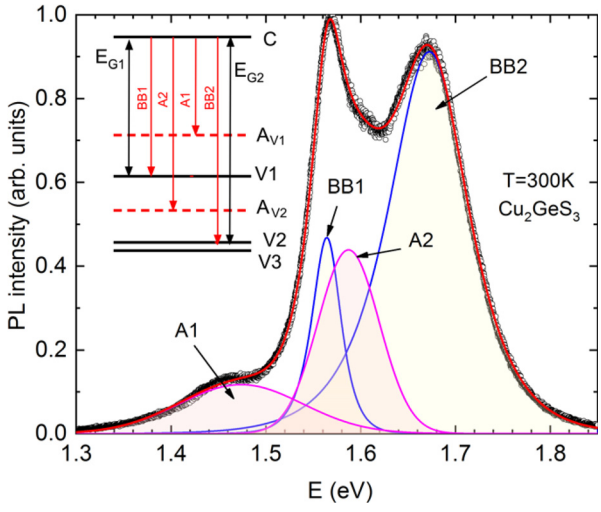

FIG. 2. Fitting result of the PL spectrum measured from type B microcrystal. The inset shows the origin of detected PL peaks.

TABLE I. Fitting parameters for four different PL bands measured from type B microcrystal.

PL band	Shape	E_{max} (eV)	FWHM (eV)
BB2	AHS	1.673	0.101
A2	Gauss	1.587	0.075
BB1	AHS	1.564	0.036
A1	Gauss	1.474	0.153

is expected given the involvement of the V2 and V3 valence bands that are separated by 0.02 eV.[13] While the relative intensity of the PL bands varies among type B microcrystals, the shape of the PL spectra does not vary significantly, see Fig. S5.

A2 and BB2 had an energy difference of roughly 0.09 eV. The BB1 and A1 bands also showed the same separation. It indicates that both the V1 and V2 valence bands are coupled to the same acceptor level with a depth of 90 meV. Further research is necessary to determine the origin of this acceptor level, which is currently unknown. At the same time in $Cu_2Ge(S_{0.4}Se_{0.6})_3$ crystals, we found the acceptor defect $E_A = 76$ meV, which is likely due to either the antisite Cu_{Ge} defect or the S/Se interstitial defect.[15] Cu_2GeSe_3 also had a deeper acceptor $E_A = 90$ meV.[18] If the acceptor level can couple strongly with both split bands, it may appear also in the higher-energy bandgap. This could happen if the wavefunctions corresponding to both bands have substantial overlap or symmetry matching with the acceptor level. As a result, the acceptor levels can take part in transitions related to both band gaps through hybridization or resonance. There are examples in the study of semiconductor physics, where an acceptor level has been observed also in the higher-energy bandgap due to valence band splitting. One example is $CuGaTe_2$ crystals, where the acceptor level was also detected in the higher-energy bandgap.[19] Similar situation was found in magnesium doped GaN.[20] Shallow acceptor resonance states were also detected in Ge and Si.[21,22]

One well-known technique for characterizing optical and electronic losses in solar cell devices is quantum efficiency measurement. Klenk and Schock's approximation can be used to determine the bandgap energy E_G from the low-energy side of the EQE curve, which is close to the bandgap energy $E \approx E_G$,[23]

$$EQE \approx K\alpha L_{eff} \approx A(E-E_G)^{1/2}/E,$$

where constant A includes all energy independent parameters, $L_{eff} = w + L_d$ is the effective diffusion length of minority carriers, L_d is their diffusion length in the absorber material, w is the width of the depletion region, and α is the absorption coefficient of the absorber material. The constant K is unity in absolute measurements. Consequently, a value E_G can be determined from a plot of $(E^*EQE)^2$ vs E at the low energy side of the EQE spectrum.

The bandgap value of 1.675 eV, corresponding to E_{G2}, was determined using the $(E^*EQE)^2$ vs E plot in Fig. 3(a). Considering that EQE behavior is typically caused by the lowest bandgap, the outcome is rather unexpected. The type B crystal's PL spectrum also demonstrates that the BB2 band's intensity is greater than the BB1 band's, see Fig. 2. This could indicate that the upper valence band V1 has a comparatively low hole density. Nevertheless, further research is necessary to address this issue.

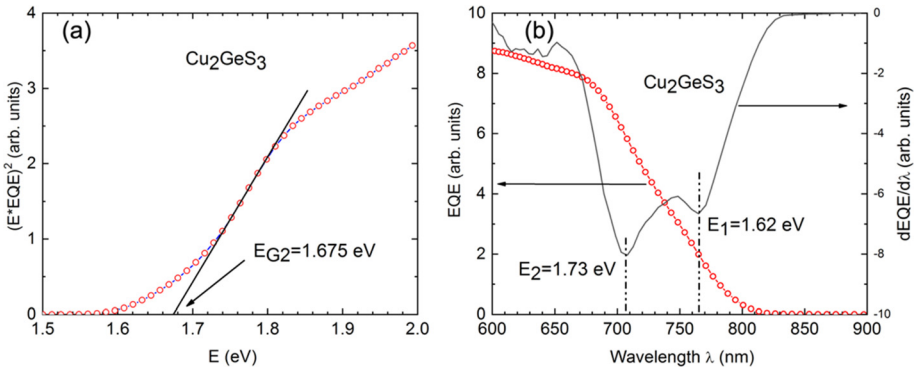

FIG. 3. (a) Bandgap extraction by plotting $(EQE^{*}E)^2$ vs E. The extrapolation of the curve to $E^{*}EQE = 0$, which gives $E_{G2} = 1.675$ eV, is indicated by the black straight line; (b) $dEQE/d\lambda$ graph showing 2 minima at 1.62 and 1.73 eV.

The derivative of the EQE spectrum [Fig. 3(b)] results in two distinct peaks, split by 0.11 eV. The inflection point minima are at 1.62 and 1.73 eV. Both minima are at about 55 meV higher energy than corresponding E_G values. Similar results were obtained also from absorption[13] and EQE measurements.[10] The slightly higher energy position of the derivative minima is typical and indicates that estimating bandgap energies from $dEQE/d\lambda$ graphs can be quite unreliable. Figure 4 compiles all the experimental data collected in this paper. Unfortunately, the dominance of E_{G2} prevented us from measuring E_{G1} from EQE data; however, our model indicates that E_{G1} must be 1.564 eV.

In conclusion, room-temperature PL, Raman, and EQE spectra of Cu_2GeS_3 microcrystals grown in molten LiI salt were analyzed. There were two types of crystals found: A and B. The PL spectra of type B crystals were composed of four distinct PL bands, whereas type A crystals displayed a PL band at 1.57 eV and a weak band at about 1.68 eV. Raman spectra of both types were also slightly different. Two band gaps were found: $E_{G1} = 1.564$ eV and $E_{G2} = 1.675$ eV. The former is associated with the upmost valence band V1, while the latter is associated with the spin–orbit split V2 valence band. It was discovered that the spin–orbit splitting energy was 0.11 eV. It was demonstrated that the V1 and V2 valence bands are connected to the same acceptor level at a depth of 90 meV. Through hybridization or resonance, this acceptor level participates in transitions associated with both band gaps. A bandgap energy was determined by EQE curve analysis. Based on these measurements, we found that the bandgap energy was 1.675 eV, meaning that the lowest valence band V2 determines the absorption close to the band edges.

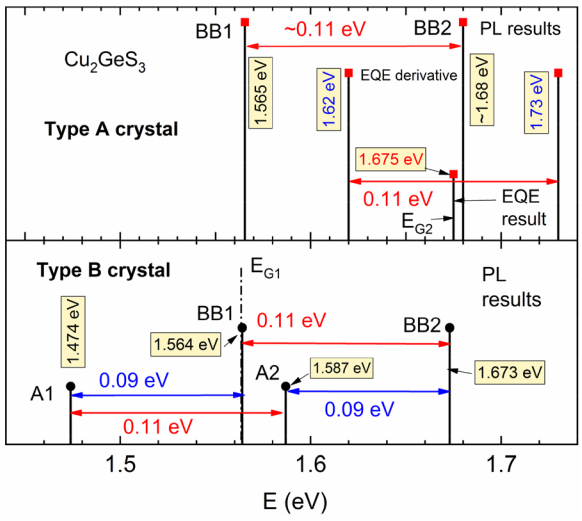

FIG. 4. Detailed overview of detected critical positions of PL peaks, EQE derivative minima, and E_G values for type A and type B microcrystals.

See the supplementary material for additional figures.

This work was supported by the European Union through the European Regional Development Fund, Project TK210, and by the Estonian Research Council under Grant No. PRG1023, and the research was conducted using the NAMUR+ core facility funded by the Estonian Research Council (TT13).

AUTHOR DECLARATIONS

Conflict of Interest

The authors have no conflicts to disclose.

Author Contributions

Jüri Krustok: Conceptualization (lead); Data curation (lead); Formal analysis (lead); Investigation (lead); Writing – original draft (lead). **Reelika Kaupmees:** Formal analysis (supporting); Investigation (supporting). **Joel Kokla:** Formal analysis (supporting). **Marit Kauk-Kuusik:** Resources (equal); Writing – review & editing (supporting).

DATA AVAILABILITY

The data that support the findings of this study are available from the corresponding author upon reasonable request.

REFERENCES

[1]W. Bao, F. Qiu, and S. Bai, J. Phys. Conf. Ser. **2578**, 012013 (2023).
[2]P. Ramasamy and J. Kim, Chem. Asian J. **10**, 1468 (2015).
[3]B. Kada, B. Karima, B. Nabil, B. Abdelkader, B. Samir, A. Charef, and B. Souheil, Ann. West Univ. Timisoara, Phys. **66**, 62 (2024).
[4]X. Jin, L. Zhang, G. Jiang, W. Liu, and C. Zhu, Sol. Energy Mater. Sol. Cells **160**, 319 (2017).
[5]Y. Matsumoto, N. Aihara, N. Saito, and K. Tanaka, Mater. Lett. **194**, 16 (2017).
[6]N. Aihara, Y. Matsumoto, and K. Tanaka, Phys. Status Solidi **254**, 1700118 (2017).
[7]Y. Kim and I.-H. Choi, J. Alloys Compd. **770**, 959 (2019).

[8]X. Li, K. Timmo, M. Grossberg, M. Pilvet, R. Kaupmees, J. Krustok, K. Muska, V. Mikli, and M. Kauk-Kuusik, Thin Solid Films **742**, 139053 (2022).
[9]H. Araki, M. Yamano, G. Nishida, A. Takeuchi, N. Aihara, and K. Tanaka, Phys. Status Solidi (c) **14**, 3 (2017).
[10]E. V. C. Robert, J. de Wild, D. Colombara, and P. J. Dale, in *Thin Films for Solar and Energy Technology VIII*, edited by M. J. Heben and M. M. Al-Jassim (SPIE, 2016), p. 993607.
[11]L. K. Samanta, Phys. Status Solidi **100**, K93 (1987).
[12]H. Araki, K. Chino, K. Kimura, N. Aihara, K. Jimbo, and H. Katagiri, Jpn. J. Appl. Phys. **53**, 05FW10 (2014).
[13]J. de Wild, E. Kalesaki, L. Wirtz, and P. J. Dale, Phys. Status Solidi RRL **11**, 1600410 (2017).
[14]M. Kauk-Kuusik, K. Timmo, M. Pilvet, K. Muska, M. Danilson, J. Krustok, R. Josepson, V. Mikli, and M. Grossberg-Kuusk, J. Mater. Chem. A **11**, 23640 (2023).
[15]J. Krustok, R. Kaupmees, X. Li, M. Kauk-Kuusik, and M. Grossberg, AIP Adv. **11**, 3 (2021).
[16]J. Krustok, R. Kaupmees, R. Jaaniso, V. Kiisk, I. Sildos, B. Li, and Y. Gong, AIP Adv. **7**, 065005 (2017).
[17]J. Krustok, R. Kondrotas, R. Nedzinskas, K. Timmo, R. Kaupmees, V. Mikli, and M. Grossberg, Adv. Opt. Mater. **9**, 1 (2021).
[18]G. Marcano, G. S. Pérez, and C. Rincón, Phys. Status Solidi (b) **254**, 2 (2017).
[19]J. Krustok, M. Grossberg, A. Jagomägi, M. Danilson, and J. Raudoja, Thin Solid Films **515**, 6192 (2007).
[20]H. Przybylinska, G. Kocher-Oberlehner, and W. Jantsch, Acta Phys. Pol. A **103**, 683 (2003).
[21]R. Buczko and F. Bassani, Phys. Rev. B **45**, 5838 (1992).
[22]S. Zwerdling, K. J. Button, B. Lax, and L. M. Roth, Phys. Rev. Lett. **4**, 173 (1960).
[23]W. R. Klenk and H.-W. Schock, in Proceeding of the 12th EU PVSEC 1588 (1994).